Bull. Mater. Sci., Vol. 37, No. 7, December 2014, pp. 1597–1602. © Indian Academy of Sciences.

# $In_xGa_{1-x}N$ fibres grown on $Au/SiO_2$ by chemical vapour deposition

**A RAMOS-CARRAZCO[1,2,*], R GARCÍA[3], M BARBOZA-FLORES[3] and R RANGEL[4]**

[1]Centro de Investigación en Materiales Avanzados, S.C., Chihuahua, Chihuahua, C.P. 31108, México
[2]Departamento de Física, Universidad de Sonora, Hermosillo, Sonora, C.P. 83000, México
[3]Departamento de Investigación en Física de la Universidad de Sonora, Hermosillo, Sonora, C.P. 83000, México
[4]Facultad de Ingeniería Química, Universidad Michoacana de San Nicolás de Hidalgo, Morelia, Michoacán, C.P. 58030, México

MS received 3 July 2013; revised 29 August 2013

**Abstract.** **The growth of $In_xGa_{1-x}N$ films ($x = 0{\cdot}1$ and $x = 0{\cdot}2$) on a thin gold layer ($Au/SiO_2$) by chemical vapour deposition (CVD) at 650 °C is reported. As a novelty, the use of a Ga–In metallic alloy to improve the indium incorporation in the $In_xGa_{1-x}N$ is proposed. The results of high quality $In_xGa_{1-x}N$ films with a thickness of three micrometres and the formation of microfibres on the surface are presented. A morphological comparison between the $In_xGa_{1-x}N$ and GaN films is shown as a function of the indium incorporation. The highest crystalline $In_xGa_{1-x}N$ films structure was obtained with an indium composition of $x = 0{\cdot}20$. Also, the preferential growth on the (002) plane over $In_{0.2}Ga_{0.8}N$ was observed by means of X-ray diffraction. The thermoluminescence (TL) of the $In_xGa_{1-x}N$ films after beta radiation exposure was measured indicating the presence of charge trapping levels responsible for a broad TL glow curve with a maximum intensity around 150 °C. The TL intensity was found to depend on composition being higher for $x = 0{\cdot}1$ and increases as radiation dose increases.**

**Keywords.** **Nitride of group-III; indium–gallium nitride; chemical vapour deposition.**

## 1. Introduction

Nitrides of group-III (GaN–InN–AlN) have gained attention due to their potential in optoelectronic applications such as laser diodes (Ponce and Bour 1997), solid-state lighting (Morgan and Zhizhen 2002), transistors (Deb *et al* 2006), UV sensors (Roberts *et al* 2002) and the new generation of solar cells (Jani *et al* 2007; Lestrade *et al* 2011).

The ternary alloy InGaN is a novel material with an important performance in the new optoelectronic devices such as light emitting diodes (LEDs) and blue laser diodes (LDs). Specifically, the InGaN acts as the active layer (Nakamura 1999) responsible to produce emissions with wavelengths at the UV, blue, green, amber and red. According to Vegard's law, it is possible to change the energy value of the band gap from 3·4 (GaN) to 0·7 eV (InN) by varying the indium composition ($0 < x < 1$) in the $In_xGa_{1-x}N$ compound, which modify the optical properties of this nitride range from UV, VIS to IR regions of the electromagnetic spectrum (McCluskey *et al* 1998; Van de Walle *et al* 1999).

Since most of the studies have been carried out for the binary materials GaN and InN, the knowledge of the InGaN ternary is still scarce and incomplete. Also, the manufacture of InGaN needs to overcome technical difficulties that currently exist, especially, the optimal growth conditions and suitable substrates to form high-quality InGaN solid-solutions (Ambacher 1998).

*Author for correspondence (antonio.ramos@cimav.edu.mx)

In the literature, there is a substantial amount of studies on the nitride compounds prepared as films and powders (García *et al* 2002). Since the GaN, InN and InGaN films have found more potential applications, the properties of these materials are widely investigated. Several growth techniques to produce these materials into films have been considered including CVD, MOCVD, MBE and MOVPE methods (Matsuoka *et al* 1992; Dupuis *et al* 1999; Red Kin *et al* 2004; Mueller *et al* 2005; Stoica *et al* 2006).

Parallel to the development of methods to obtain InGaN films, the substrate used is an essential issue, since a lattice mismatch between the substrate and the nitride may have a significant disadvantage in producing semiconductor materials with high quality and reproducibility. Commonly, sapphire (Dong-Joon *et al* 2001; Wu *et al* 2003; Hahn *et al* 2011) has been used due to its high order of symmetry and smaller lattice differences with respect to nitrides. Also, other substrates have been used to grow InGaN films such as 6H-SiC, AlN, 3C-SiC, GaAs, ZnO, $LiGaO_2$ and MgO (Liu and Edgar 2002).

From the above, it follows that the parameters influencing the growth, alloy composition, substrate and the chosen method have a decisive effect on the properties of the InGaN solutions. Thus, the multiple variables involved motivates the research and development of novel synthesis techniques to find the optimal conditions for producing high quality InGaN materials.

In the present work, the growth of $In_xGa_{1-x}N$ films with an indium composition of $x = 0{\cdot}1$ and $x = 0{\cdot}2$ using

chemical vapour deposition technique (CVD) is discussed. Also, the innovative process to produce an indium–gallium metallic alloy is presented in detail. The characterization results of XRD, TEM microscopy, SEM microscopy and TL measurements are presented. By means of scanning electron microscope, the formation of fibres on the surface of the $In_xGa_{1-x}N$ films was demonstrated. The crystalline structure of the grown $In_xGa_{1-x}N$ was determined by X-ray diffraction and compared to the well-known crystallographic properties of the GaN wurtzite phase. The thermoluminescence response of the $In_xGa_{1-x}N$ films and substrate used was measured in order to investigate the existence of charge carriers trapping levels inside the band gap of $In_xGa_{1-x}N$.

## 2. Experimental

### 2.1 *Growth procedure: alloy formation and CVD system*

Before deposition, the $In_x$–$Ga_{1-x}$ metallic alloys were formed with two varied compositions of $x = 0{\cdot}1$ and $x = 0{\cdot}2$ by a heat treatment. Figure 1 shows a diagram of the vertical steel reactor and main components used to produce the alloy. First, the metals are weighed and placed into a small aluminum oxide boat inside the vertical chamber as shown in figure 1, followed by vacuum at $10^3$ Pa and heated in the range of 200−260 °C. Then, a $N_2$ flux of 200 sccm is provided to fill the chamber at atmospheric pressure and a mechanical vibration system is also activated. The time of this process was set for 1 h. Finally, the In–Ga metallic alloys are removed from the ceramic boat and placed in the corresponding container of the CVD reactor. In the case of $In_xGa_{1-x}N$ with an indium composition of $x = 0$, the gallium metallic is not exposed to heat treatment.

The chemical vapour deposition system consists of a horizontal furnace made of a quartz tube of $2\frac{1}{2}''$ diameter divided into three thermal zones. Two concentric quartz tubes of $\frac{3}{4}''$ diameter allow the entry of the precursor gases of high purity ammonia ($NH_3$) and nitrogen ($N_2$) as carrier gas. After the formation of every metallic alloy, each one was placed into one of the inner quartz tubes at the zone 2 (630 °C) of the furnace. Out of the furnace, ammonia chloride ($NH_4Cl$) was introduced in the same tube at the entrance of zone 1. Then, a substrate silicon dioxide ($Au/SiO_2$) previously coated with a thin layer of gold (∼50 nm) is placed at zone 2 and a heat treatment is applied for 1 h in a vacuum atmosphere. Then, an ammonia flux of 350 and 200 sccm of nitrogen are provided. At the same time, the $NH_4Cl$ is moved using a magnetic manipulator in steps of 30 mm, each 5 min, toward the zone 1 at 900 °C (see figure 1b). The growth process was performed under pressure of 254 Torr during 15 min. Finally, the same procedure was applied to every Ga–In alloys with different indium concentrations on each $In_xGa_{1-x}N$ film. In the case of $In_xGa_{1-x}N$ with an indium composition of $x = 0$, the gallium metallic is only weighed and placed in zone 2.

### 2.2 *Characterization*

The morphology of synthesized InGaN films was characterized by means of a Jeol 5300 scanning electron microscope. High resolution images were taken with a Tecnai Philips F20 transmission electron microscope. The X-ray diffraction characterization was performed with a D500 Siemens diffractometer in a range of 10–70° ($2\theta$) at room temperature using a wavelength of 1·54 Å, at 45 kV and 30 mA. The thermoluminescence characterization was performed in a Risø TL/OSL-DA-20 system provided with a $^{90}Sr$–$^{90}Y$ beta radiation source with a dose rate of 0·1 Gy $s^{-1}$. The TL glow curves were obtained from 30 to 400 °C at a heating rate of 1·0 °C $s^{-1}$ and using exposure doses from 12·8 to 102·4 Gy. The thermally-stimulated luminescence (TL) is detected by a photomultiplier tube (EMI 9235QB) with a maximum detection efficiency between 200 and 400 nm.

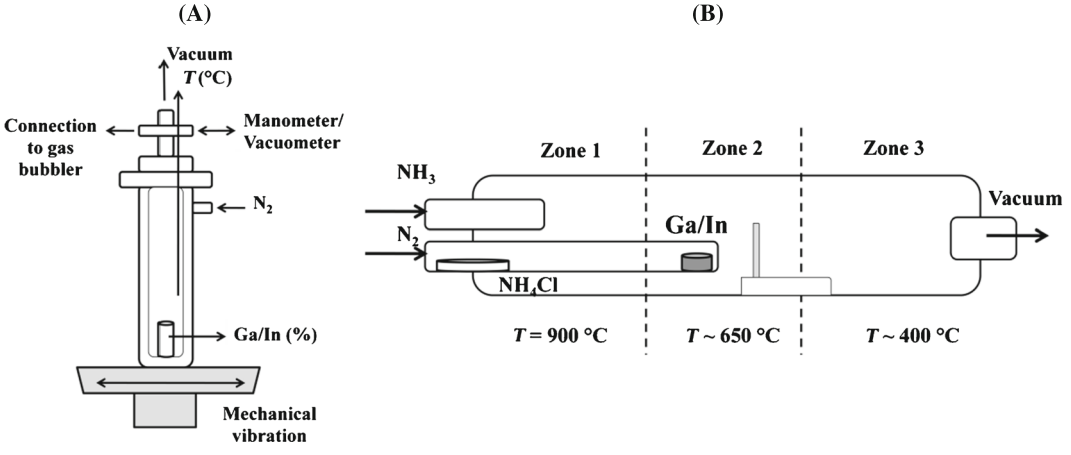


**Figure 1.** Schematic diagrams of the two stages of indium–gallium nitride growth. **(A)** Small reactor used for In–Ga alloy formation and **(B)** horizontal CVD reactor used for the $In_xGa_{1-x}N$ growth.

## 3. Results and discussion

### 3.1 *X-ray diffraction*

The diffractogram obtained for three $In_xGa_{1-x}N$ ($x = 0$, $x = 0{\cdot}1$ and $x = 0{\cdot}2$) films with the crystallographic features of a hexagonal wurtzite is presented in figure 2. The first $In_xGa_{1-x}N$ ($x = 0$) sample was grown to establish a comparison with the synthesized ternary alloys. In such a case, the main planes (002), (100) and (101) are indexed using the location of XRD peaks in the GaN phase, according to the ICDD card database 00-050-0792. From figure 2, the XRD pattern shows a better crystalline state for the case of pure GaN film with a higher relative intensity on the (002) plane. As the indium concentration increases, a shift of $2\theta$ position to minor angles and broadening of the main peaks is observed with a maximum change of $\Delta(2\theta) = 0{\cdot}10°$, between $In_{0{\cdot}1}Ga_{0{\cdot}9}N$ and $In_{0{\cdot}2}Ga_{0{\cdot}8}N$ samples. This result confirms a change of indium content according to the corresponding $2\theta$ positions of the same crystallographic planes (002), (100) and (101) with respect to that of InN–GaN. Therefore, the formation of $In_xGa_{1-x}N$ phase is obtained in the range of $2\theta$ between 31 and 37° approximately (Ramos-Carrazco *et al* 2011).

As a degree of crystalline quality, the full-width at half-maximum (FWHM) is calculated for each $In_xGa_{1-x}N$ sample. The GaN film presents the higher crystallinity, which can be demonstrated with the lower value of FWHM = 0·15° for $x = 0$ measured in the $In_xGa_{1-x}N$ specimens. In comparison, the $In_{0{\cdot}1}Ga_{0{\cdot}9}N$ and $In_{0{\cdot}2}Ga_{0{\cdot}8}N$ films show an increase in the FWHM values of 0·94° and 0·66°, respectively. Despite the compositional modulation of the peaks on the $In_xGa_{1-x}N$ samples, the nitride with an indium content of $In_{0{\cdot}2}Ga_{0{\cdot}8}N$ presents a higher crystalline quality compared to the $In_{0{\cdot}1}Ga_{0{\cdot}9}N$ film. Also, the average size of the particles was calculated at the most intense peak (002) by the Scherrer's equation ($t = 0{\cdot}9\lambda/\beta\cos\theta$). The average size obtained for the $In_xGa_{1-x}N$ samples show a significant decrease between GaN and InGaN phases. For the GaN, the calculated size of particle was 52 nm and, 8 and 12 nm for the $In_{0{\cdot}1}Ga_{0{\cdot}9}N$ and $In_{0{\cdot}2}Ga_{0{\cdot}8}N$ samples, respectively.

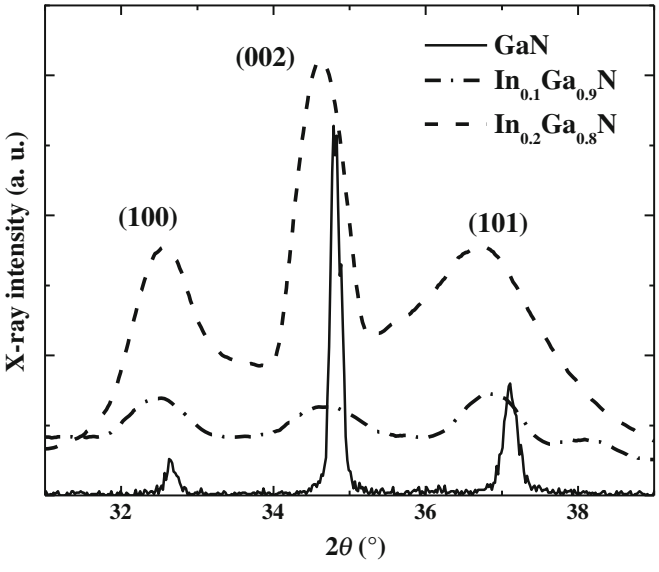


**Figure 2.** X-ray diffractogram patterns of $In_xGa_{1-x}N$ samples: **(A)** GaN, **(B)** $In_{0{\cdot}1}Ga_{0{\cdot}9}N$ and **(C)** $In_{0{\cdot}2}Ga_{0{\cdot}8}N$.

### 3.2 *Electron microscopy*

The different surface morphologies of the $In_xGa_{1-x}N$ films are shown in figure 3. From figure 3(A), the formation of multiple GaN microfibres with lengths superior to 20 $\mu$m is shown. In $In_{0{\cdot}1}Ga_{0{\cdot}9}N$ (see figure 3B) and $In_{0{\cdot}2}Ga_{0{\cdot}8}N$ (see figure 3C) samples, a similar growth pattern with a different distribution was obtained on the surface. Also, it can be observed that a dependence of the thickness on the $In_xGa_{1-x}N$ fibre with the increment of indium content. Some morphological formations similar to the present work have been reported in the research of GaN as nanowires (Devi *et al* 2005), using similar methods of growth (Carbajal *et al* 2011) and even other metals such as nucleation centres (Zhou *et al* 2012). There is a strong formation of GaN structures like wires and rods, as in the present micro-fibres, when a metal thin layer is used as nucleation catalyst. Compared to reported GaN nanowires, where the thickness of the metallic coating is between 10 and 15 nm (Cai *et al* 2009); in this work, the $In_xGa_{1-x}N$ films were grown on a layer of about 50 nm. However, the importance of this layer lies in the formation of nucleation sites created after the heat treatment on the substrate. Therefore, it is clear that the catalyst metal layer is directly dependent on the dimensions of the applied coating.

TEM microscopy results for the $In_{0{\cdot}1}Ga_{0{\cdot}9}N$ sample are presented in figure 3(D). From the high resolution image, two crystallographic planes were identified as (002) and (101) corresponding to the interplanar distances of 2·59 and 2·43 Å. Using the software digital micrograph, the theoretical interplanar distances were compared to that of the crystallographic ICDD file relative to GaN.

### 3.3 *TL measurements*

Many potential and novel applications of GaN–InN–AlN as sensors, LED, transistors, solar cells and other optoelectronic devices depend on the charge-transport properties of the material used. The device performance is strongly dependent on the number of intrinsic defects contents and those defects induced by impurities during synthesis of a specific compound. It is well known that CVD methods may produce a great amount of crystalline defects and may also introduce impurity defects during the growth process. Thermally-stimulated luminescence, usually called thermoluminescence (TL), is a very sensitive technique to detect defects at extremely low concentration levels. The TL phenomenon is observed in samples previously exposed to ionizing or non-ionizing radiation source, which creates

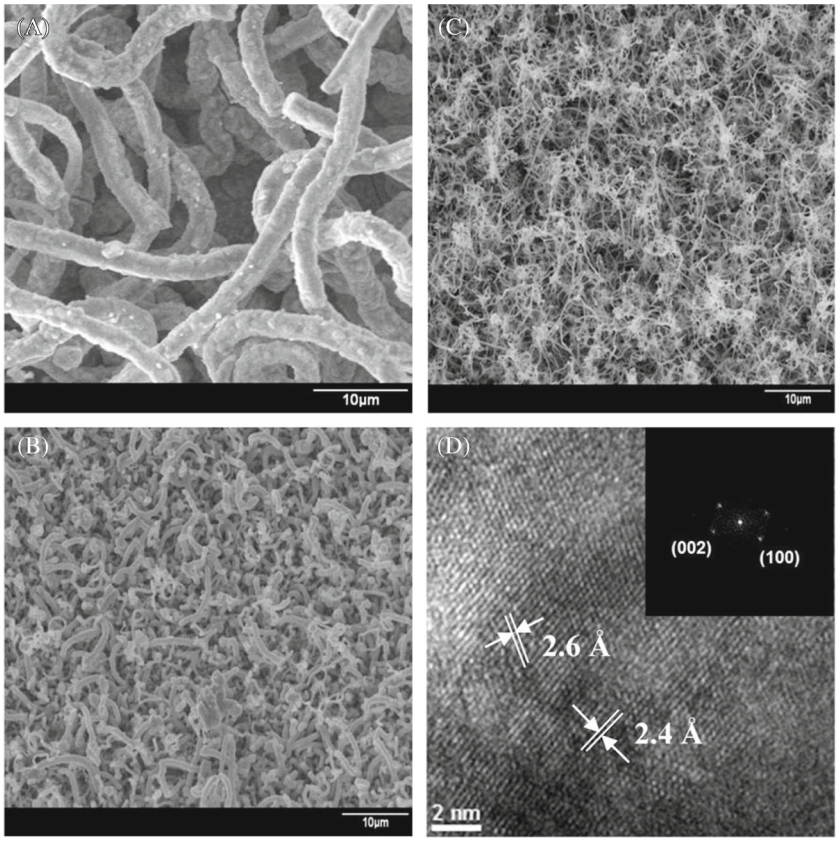


**Figure 3.** SEM and TEM images of the $In_xGa_{1-x}N$ samples grown by chemical vapour deposition: **(A)** GaN, **(B)** $In_{0.1}Ga_{0.9}N$, **(C)** $In_{0.2}Ga_{0.8}N$ and **(D)** high resolution TEM image of the $In_{0.1}Ga_{0.9}N$.

electron hole pairs charge carriers that may be trapped by localized trapping levels inside the band gap and related to the defects content in the sample under investigation. Usually, some charge carriers remain trapped at room temperature and after thermal stimulation, they are freed and may recombine radiatively with a recombination centre. The resulting light intensity as a function of temperature during heating gives rise to TL glow curve which is characteristic of the material. The TL glow curve may give information about the existence of the trapping levels related to the existence of defects and the depth or activation energies of localized trapping levels inside the band gap of the materials. In the present case, we have used TL to qualitatively assess the effect of the CVD process on the defect formation during growing.

Figure 4 exhibits the TL glow curve of $In_xGa_{1-x}N$ ($x = 0{\cdot}1$ and $x = 0{\cdot}2$) specimens after exposed to beta radiation at different doses. The TL glow curve is a broad band centred around 150 °C in which the intensity increases as the dose increases from 25·6 to 102·4 Gy being higher for $x = 0{\cdot}1$ composition. We observe that the position of the TL maximum shifts to lower temperature as the dose increases suggesting that a second-order TL process is taking place. Physically, second-order kinetics implies the possibility of retrapping during the thermal excitation period meaning that a significant number of charge carriers are retrapped before they recombine. This second-order process typically gives rise to a wider and more asymmetrical, like bell-shaped TL glow curve, as opposed to the asymmetrical and wider on the low temperature side than on the high temperature side characteristic of first-order kinetics process occurring under slow retrapping probability. However, establishing the accurate kinetics process occurring in $In_xGa_{1-x}N$ may involve a more detailed work using computer glow curve deconvolution (CGCD) and fitting procedures that are far from the qualitative scope and objectives of the present work.

Given the variety of defects that one might expect to find in crystalline and highly amorphous $In_xGa_{1-x}N$ grown by CVD technique, it is convenient to examine the defects related to the $Au/SiO_2$ substrates used to deposit in the $In_xGa_{1-x}N$ film, since it is evident that the measured TL is due to the substrate and the thin gold layer and the nitride top layer. In order to evaluate separately the TL response of $In_xGa_{1-x}N$ and $In_xGa_{1-x}N/Au/SiO_2$ multi-layers, the $In_{0.1}Ga_{0.9}N$ film was removed from the substrate with hydrofluoric acid (HF) and a measure of the TL was performed exposed to extremely high 360 Gy dose of beta radiation. The TL glow curve of the $In_{0.1}Ga_{0.9}N$ with the substrate removed (free-standing) is presented in figure 5. Note that the isolated $In_{0.1}Ga_{0.9}N$

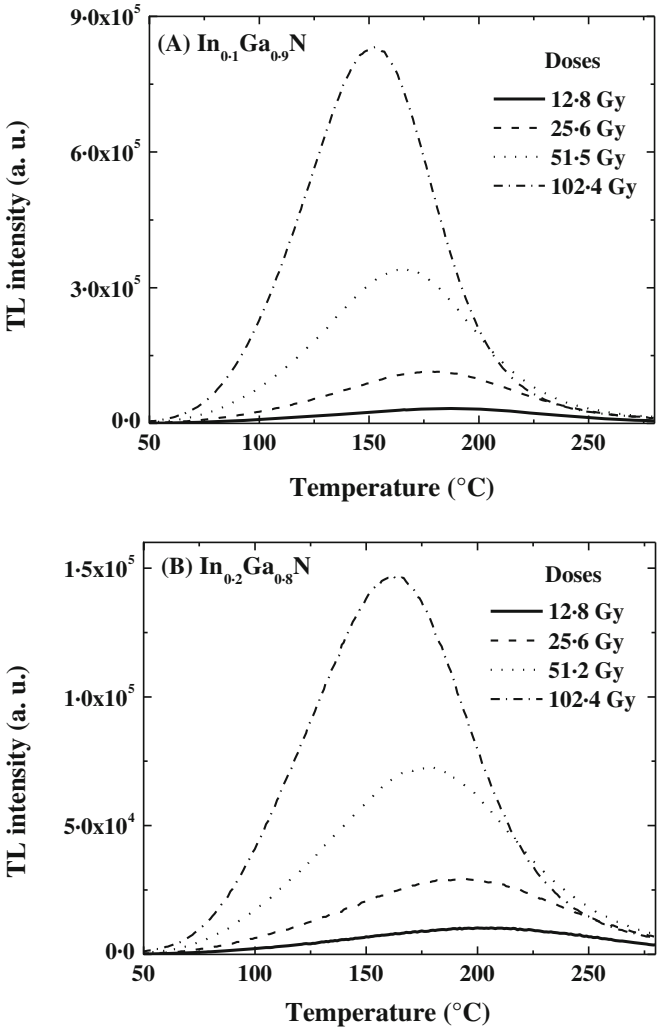


**Figure 4.** Thermoluminescence glow curve of **(A)** $In_{0.1}Ga_{0.9}N$ and **(B)** $In_{0.2}Ga_{0.8}N$ samples exposed to beta radiation at different doses.

layer shows a significant decrease of two order of magnitude of the TL signal in comparison with the multi-layer TL response. The free-standing $In_{0.1}Ga_{0.9}N$ TL glow is composed of several overlapped peak components located at the 50–350 °C temperature range with maximum peaks around 150 and 230 °C. This TL glow curve is characteristic of a continuum trap distributions in a region of two-localized relatively deep main trapping levels. Notice that the TL was obtained on a high dose of 360 Gy compared to the doses exposure given to the multilayer InGaN; therefore, been negligible for practical purposes. We have not observed spectral response of the TL; however, the maximum detection efficiency of the TL detector is between 200 and 400 nm, which concise with the emission range of the InGaN.

It is pertinent to recall that Au has no TL after irradiation. Therefore, the observed TL shown in figure 4 may be mainly due to $SiO_2$ and some impurities and defects produced during the growth process. In any case, the most important issue is related to the fact that the main contribution to the TL comes

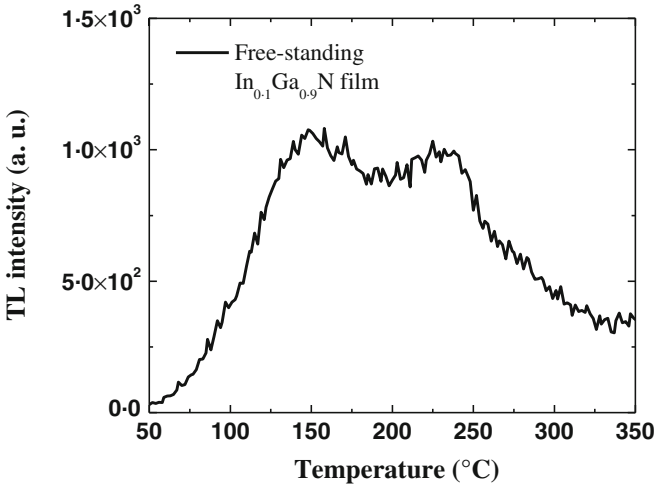


**Figure 5.** TL signal of free-standing $In_{0.1}Ga_{0.9}N$ layer exposed to 360 Gy of beta radiation.

from the substrates and it could be of importance for specific device application of the $In_{0.1}Ga_{0.9}N$ material which may or may not require some substrate.

## 4. Conclusions

We have provided evidence that Au layer affect on the growth of $In_xGa_{1-x}N$ films promoted the formation of microfibres and that the thickness of the metallic layer has strong dependence on the dimensions of the resulting nucleation sites. Also, the indium incorporation in the $In_xGa_{1-x}N$ phase directly affects in the decrease of the fibre diameter while preserving the hexagonal crystalline phase. Therefore, the size of the $In_xGa_{1-x}N$ fibres depends on the indium composition and the seed particles created by the annealing of the gold layer. The sample of $In_{0.2}Ga_{0.8}N$ showed higher crystallinity than the $In_{0.1}Ga_{0.9}N$ and its quality is comparable to that of the GaN film used as reference in this work. It was shown by thermoluminescence that the number of localized charge trapping levels is significantly lower in free-standing $In_xGa_{1-x}N$ layers in comparison with the $InGaN/Au/SiO_2$ multilayer structure. The CVD reactor used in this work demonstrates a real improvement on the indium incorporation and the growth of high quality microstructured $In_xGa_{1-x}N$. Future work involves the use of metallic alloys with higher indium composition ($x > 0{\cdot}2$) in order to decrease the $In_xGa_{1-x}N$ band gap and the defect distributions which are of importance for optoelectronic, sensors and photovoltaic applications.

## Acknowledgements

Authors gratefully acknowledge to Universidad Michoacana and Universidad de Sonora for the technical facilities provided. This research work was supported by CONACYT (project #102671).

## References


Ambacher O 1998 *J. Phys. D: Appl. Phys.* **31** 2653

Cai X M, Ye F, Jing S Y, Zhang D P, Fan P and Xie E Q 2009 *J. Alloys Compd.* **467** 427

Carbajal G G, Soto G, Fisher A M and Contreras O E 2011 *J. Cryst. Growth* **319** 19

Deb P, Kim H, Qin Y, Lahiji R, Oliver M, Reifenberger R and Sands T 2006 *Nano Lett.* **6** 2893

Devi A, Schmid R, Muller J and Fischer R A 2005 *Top Organomet. Chem.* **9** 49

Dong-Joon K, Yong-Tea M, Keun-Man S, In-Hwan L and Seon-Ju P 2001 *J. Electron. Mater.* **30** 99

Dupuis R D, Grudowski P A, Eiting C J and Park J 1999 *Semiconductors* **33** 965

García R, Hirata G A, Farias M H and McKittrick J 2002 *Mater. Sci. Eng.* **B90** 7

Hahn C, Zhaoyu Z, Fu A, Cheng Hao W, Yun Jeong H, Gargas D J and Yang P 2011 *ACS Nano* **5** 3970

Jani O, Ferguson I, Honsberg C and Kurtz S 2007 *Appl. Phys. Lett.* **91** 132117

Lestrade M, Li Z Q, Xiao Y G and Simon Li Z M 2011 *Opt. Quant. Electron.* **42** 699

Liu L and Edgar J H 2002 *Mater. Sci. Eng.* **R37** 61

Matsuoka T, Yoshimoto N, Sasaki T and Katsui A 1992 *J. Electron. Mater.* **21** 157

McCluskey M D, Van de Walle C G, Master C P, Romano L T and Johnson N M 1998 *Appl. Phys. Lett.* **72** 2725

Morgan N N and Zhizhen Y 2002 *J. Micro. Optoelectron.* **2** 52

Mueller A H, Petruska M A, Achermann M, Werder D J, Akhadov E A, Koleske D D, Hoffbauer M A and Klimov V I 2005 *Nano Lett.* **5** 1039

Nakamura S 1999 *Semicond. Sci. Technol.* **14** R27

Ponce F A and Bour D P 1997 *Nature* **386** 351

Ramos-Carrazco A, Chaikina E, Contreras O E, Barboza-Flores M and Garcia R 2011 *Revista Mexicana de Fisica* **57** 7

Red Kin A N, Tatsi V I, Makovei Z I, Gruzintsev A N and Yakimov E E 2004 *Inorg. Mater.* **40** 1197

Roberts J C, Parker C A, Muth J F, Leboeuf S F, Aumer M E, Bedair S M and Reed M J 2002 *J. Electron. Mater.* **31** L1

Stoica T, Meijers R J, Calarco R, Richter T, Sutter E and Luth H 2006 *Nano Lett.* **6** 1541

Van de Walle C G, McCluskey M D, Master C P, Romano L T and Johnson N M 1999 *Mater. Sci. Eng.* **B59** 274

Wu J, Walukiewicz W, Yu K M, Shan W, Ager III J W, Haller E E, Lu H, Schaff W J, Metzger W K and Kurtz S 2003 *J. Appl. Phys.* **94** 6477

Zhou X, Chesin J, Crawford S and Gradecak S 2012 *Nanotechnol.* **23** 285603